NEXT GENERATION, WAVEFORM BASED THREE-DIMENSIONAL MODELS AND METRICS TO IMPROVE NUCLEAR EXPLOSION MONITORING IN THE MIDDLE EAST

Brian Savage[1], Daniel Peter[2], Brian Covellone[1] Arthur Rodgers[3], and Jeroen Tromp[2]

University of Rhode Island[1], Princeton University[2], and Lawrence Livermore National Laboratory[3]

Sponsored by the Air Force Research Laboratory and the National Nuclear Security Administration

Award Nos. FA8718-08-C-0009[1,2] and DE-AC52-07NA27344[3]
Proposal No. BAA08-79

ABSTRACT

Improvements to current wave speed models of the Middle East requires confidence in sources and recordings, along with a methodology to directly improve 3D wave speed models. Recordings of seismic waves traversing the region from Tibet to the Red Sea are the principal metric in guiding improvements to the current wave speed model using adjoint waveform tomography. To avoid a mapping of source errors, including incorrect depths and faulting mechanisms, into the new wave speed model, a rigorous characterization of each source within the current wave speed model was undertaken. Source depths and paths near nodal planes are particularly error prone as small changes may severely affect the resulting wavefield. As these sources have been evaluated, regions requiring refinement will be highlighted using adjoint tomography methods based on spectral-element simulations (Komatitsch and Tromp, 1999).

Following source evaluations using teleseismic body waves (Kikuchi and Kanamori, 1982) and regional surface and body waves (Zhao and Helmberger, 1994), we reinterpreted a large, well-recorded subset of 201 events (1990–2007) through a direct comparison between data and synthetics based upon a centroid moment tensor inversion (Liu et al., 2004). Evaluation was done using both a 1D reference model (Dziewonski and Anderson, 1981) at periods greater than 80 seconds and a 3D model (Kustowski et al., 2008) at periods of 25 seconds and longer. The final source reinterpretations within the 3D model define a source database and the initial starting point for the adjoint tomography. Transitioning from a 1D to 3D wave speed model shows dramatic improvements when comparisons are done at shorter periods (25 s). Synthetics from the 1D model were created through mode summation while those from the 3D model were created using the spectral-element method.

To further assess errors in source depth and focal mechanism, comparisons between the three methods were made. These comparisons help to identify problematic stations and sources that may bias the final solution. Estimates of standard errors were generated for each event's source depth and focal mechanism to identify poorly constrained events. The final, well-characterized set of sources and stations is currently used to iteratively improve the wave speed model of the Middle East. After a few iterations during the adjoint inversion process, the sources will be reexamined and relocated to further reduce mapping of source errors into structural features.

Finally, efforts continue to update the current wave speed model using adjoint tomography. Initial inversion iterations have guided the measurements, model smoothing and filtering to produce the accurate and relevant improvements to the initial model. Event kernels can now be computed "quickly" at the n-th iteration and invert for a new $(n+1)$-th wave speed model of the Middle East. As demonstrated with previous adjoint tomography experiments (Tape et al., 2009), each iteration only improves the model progressively, and relies on successive iterations to reduce variance and improve the fitting of data to synthetics. Exploiting the source database with multiple adjoint inversions at shorter and shorter periods will refine the wave speed structures of the Middle East.

OBJECTIVES

Improving models of 3D wave speeds within the greater Middle East, from the Turkish Plateau to the eastern edge of Tibet (Figure 1), will enhance our ability to discriminate between natural and man-made events, locate these events, identify source depths, and determine magnitudes. Current wave speed models of the Middle East will be improved through an adjoint tomography method (Tromp et al., 2005) by a comparison of seismic phase and amplitude data. The initial step towards our adjoint tomography model involves the development of a database of relocated and characterized set of sources and waveforms. Events were re-inverted in 1D and 3D wave speed models and agree fairly well with currently available solutions and across wave speed models. The adjoint tomography method (Tromp et al., 2005) uses full seismic waveforms as a measure of misfit of the current model iteration. Differences between data and synthetics are used to create adjoint sources and generate sensitivity kernels required to update the wave speed model. A first set of test iterations towards an improved wave speed model of the Middle East will be presented here and a final model built on the foundation of the seismic waveform database will be distributed to the community.

RESEARCH ACCOMPLISHED

Event Characterization

Using the CMT inversion methodology of Liu et al. (2004), ~200 events in the Middle East were re-characterized using the 1D PREM model (Dziewonski and Anderson, 1981) at periods of 80 seconds and longer and within a 3D wave speed model (S2.9EA) (Kustowski et al., 2008) at much shorter period, 25 seconds. Initially, the procedure of processing large amounts of data, comparing these to synthetics, and reevaluating the source parameters and locations needed to be assessed and streamlined. This procedure, accomplished through the 1D long period modeling, needed to be straightforward and able to avoid problematic areas, as the initial 3D event re-evaluation requires more demanding computational efforts. Further source evaluations in updated wave speed models will occur two to three more times during the adjoint inversion. Problematic events and stations were subsequently screened out within this procedure before building the final waveform data set. Problematic stations and waveforms with dropouts and poorly characterized amplitude responses can negatively influence a CMT inversion, and these stations were removed before any 3D CMT inversions or adjoint inversions were performed.

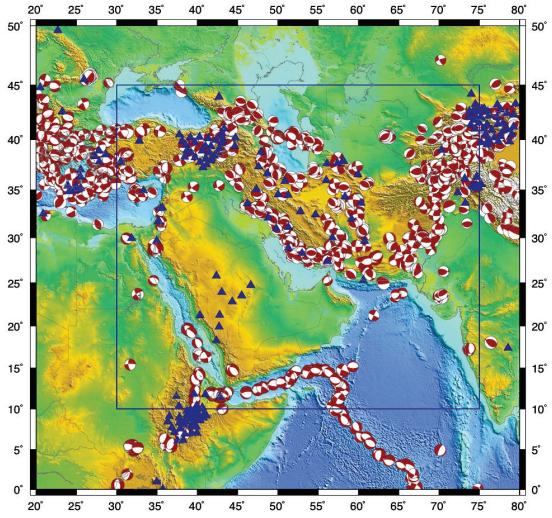

Figure 1. Map of the available sources and stations in the Middle East for the adjoint tomography inversion.

Solutions using the long period 1D model are shown in Figure 2 (left) and within the 3D wave speed model (right). Faulting parameters agree reasonably well with those from the Global CMT Project, but depths are biased towards the surface when using the 1D model. This is most likely due to the 3D model corrections used at the Global CMT Project or reduced depth sensitivity when using longer period records. However, depths compare well between the 3D solutions and the Global CMT Project. Solutions match reasonably well when using either 1D or 3D wave speed models, but the 3D wave speed synthetics use a much smaller minimum period, 25 seconds, that incorporates complicated body wave arrivals and more pronounced surface wave arrivals and dispersion.

Figure 3 displays vertical component data (black) and synthetics (red) for a single event on 2005/03/13 in the southern Zagros Mountains recorded by two stations (KURK.II and KIEV.IU) to the north. Synthetics from the 1D PREM model at long and short periods are displayed in the first two columns of Figure 3. At long periods, the data and synthetics are relatively simple, with identifiable, small amplitude body wave arrivals and much larger amplitude, fundamental mode, surface wave arrivals. Synthetics match the absolute arrivals times rather well, but

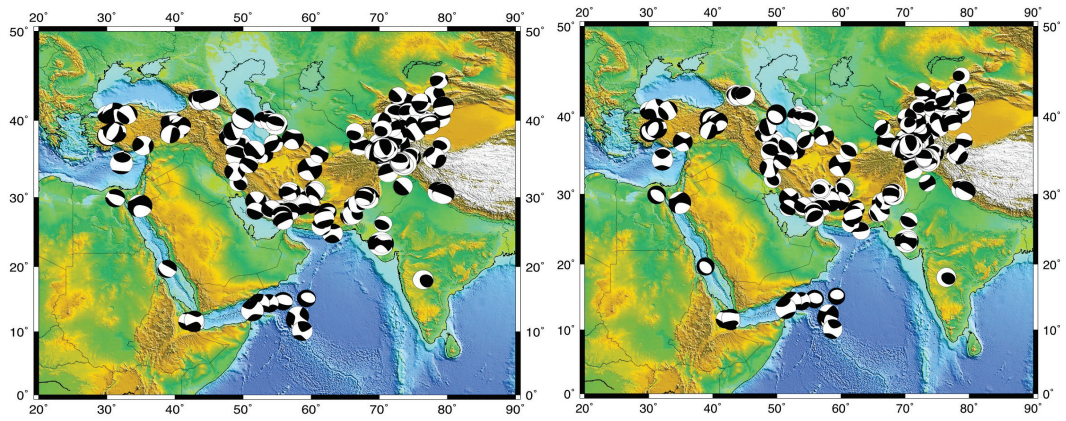

Figure 2. Comparison of solutions using a 1D wave speed model at 80 s, left, and the 3D model at 25 s, right. Fault plane solutions are constrained to be zero trace and the depth is also solved for. Solutions do not change when using either model, but depths do show systematic variation. The fault plane solution catalog includes ~200 events.

the amplitudes differ for each station at the longest period, 80 seconds. As shorter periods are included, middle column at 25 seconds, the 1D synthetics display simple arrivals but the data starts to show dispersion due to traversing the continent (see 800 to 1100 seconds for station KURK.II.LHZ and 1000 to 1400 seconds for station KIEV.IU.LHZ). Body wave arrivals also show more complex propagation as compared to the 1D synthetics, including larger amplitudes and longer duration coda (see 600 to 700 seconds for KURK.II.LHZ and 700 to 900 for KIEV.IU.LHZ in Figure 3 middle column). Simulations using the S2.9EA model (Kustowski et al., 2008) model reproduce the recorded data more closely than the 1D model at 25 seconds, Figure 3 right column. Use of the 3D wave speed model provides a more robust, shorter period estimation of the faulting parameters without losing the essential, long period estimate of the moment / magnitude. The more complex propagation paths, represented by the waveform coda in the data and now the synthetics, do not influence the estimates of source epicenter, faulting parameters, and more importantly source depth.

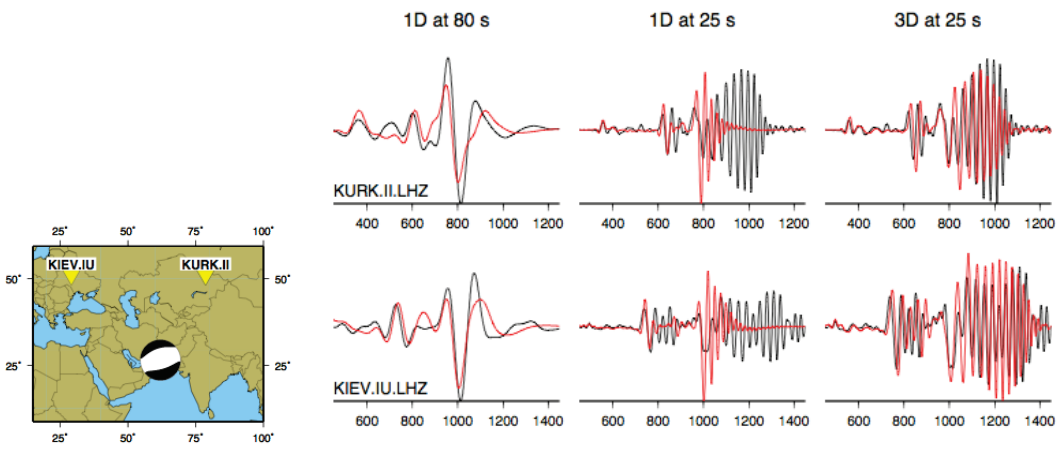

Figure 3. Comparison of vertical data (black) and synthetics (red) at 80 s and 25 s using a 1D and 3D wave speed model. The event and stations are located on the map, left. Use of the 3D wave speed model improves the match between the data and synthetics, specifically the body wave arrivals and the surface wave dispersion.

Adjoint Inversions and Model Updates

Using the discrepancies between the observed and synthetic seismograms, an event kernel can be constructed for each source solution using the adjoint method (Tromp et al. 2005). The sum of all these event kernels guides model updates of the current iteration. Measurements are made automatically between the data and synthetics using the Flexwin tool (Maggi et al., 2009), creating isolated data windows and metrics that are then used in the creation of the adjoint source. Windows, and their adjoint sources, are not constrained to any specific seismic phase or time window and only use well matched data-synthetic pairs. Adjoint sources along with the reconstructed, full synthetic wavefield are propagated in reverse time through the current iteration wave speed model to identify locations in the model requiring improvement. Interactions between the adjoint sources and the time-reversed wavefield, integrated over time, generate kernels specific to each measurement, e.g., a simple difference between the data and synthetics. Such kernels can be created using individual, isolated measurements or for each event with a large number of back-propagated adjoint sources to create event kernels. Event kernels are then summed volumetrically to produce Frechet derivates which are used to update the wave speed model.

In a first attempt, our updates to the wave speed model use a steepest descent method with tight controls on the magnitude of the update. Examples of the first two adjoint iterations to the shear wave speed model are displayed in Figure 4. The maximum change in the model update is limited to 3% based on comparisons between data and synthetics from a set of test events not used in the inversion. The shear wave speed model oscillates between the first and second inversion, Figure 4. This is most likely due to the improvement methodology, smoothing the largest differences between data and synthetics, which dominate the model update. With each iteration of these initial tests, finer scale structure begins to appear and the large-scale oscillations disappear. Successive iterations also introduce higher frequencies into the inversion not present during previous iterations.

Total updates for the shear wave speed relative to the initial model are displayed in Figure 5 with a maximum change of 5%. The oscillation seen in Figure 4 is not apparent in the total model updates indicating its source is most likely the removal of the largest data/synthetic discrepancies. As with Figure 4, more updates provide finer structure as higher-frequency signals are added to the inversion. The total misfit between the data and synthetics as measured by metrics from FLEWIN (time shift, amplitude ratio, and cross-correlation value) all show progressive

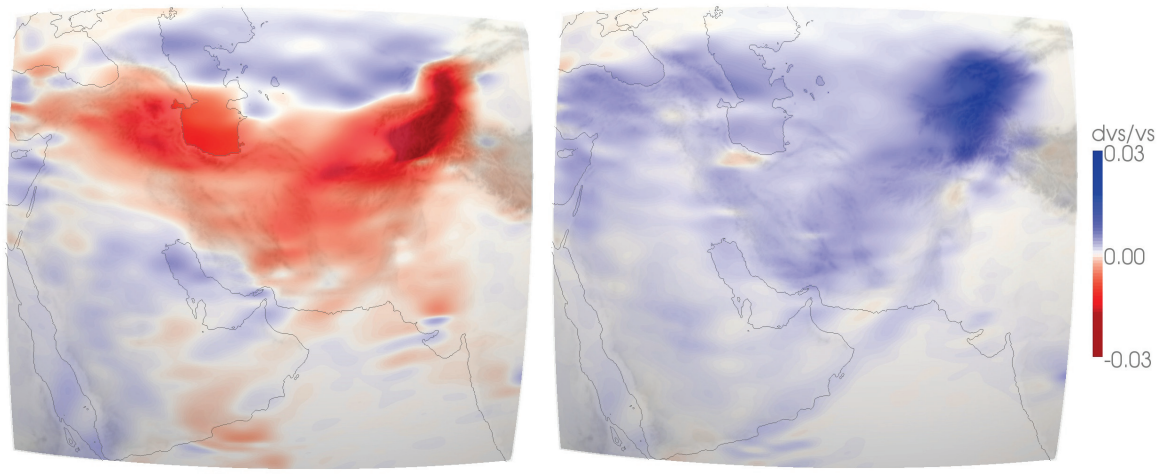

Figure 4. Adjoint model iteration updates 1 and 2, left and right, for the shear wave speed at 50 km depth. Maximum update value shown is +- 3% with blue indicating increases in wave speed.

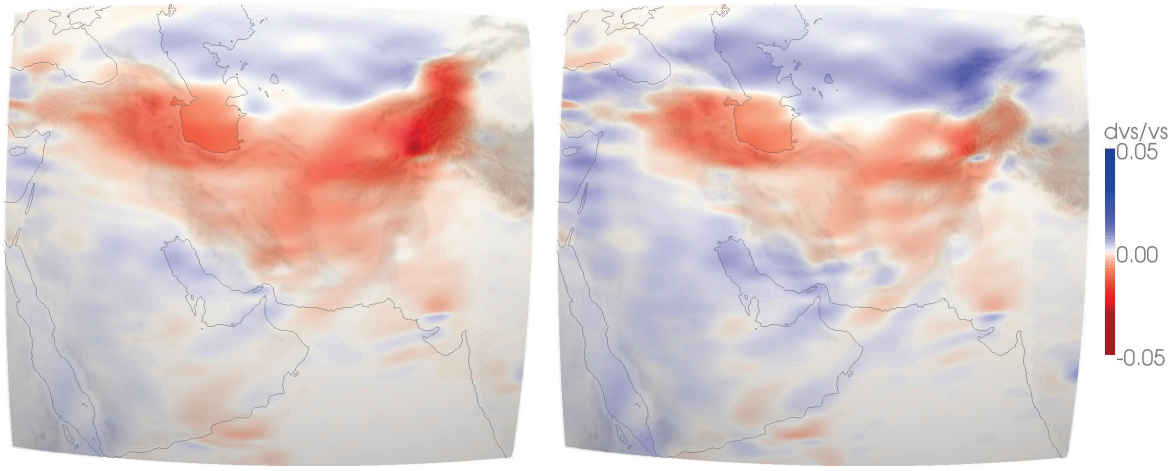

Figure 5. Adjoint model iterations 1 and 2, left and right, for the shear wave speed at 50 km depth relative to the initial 3D model. Maximum difference shown for updates is +- 5% with blue indicating faster wave speeds.

improvement to the synthetics relative to the data for each iteration.

A comparison between the total model updates and the initial model (S2.9EA) perturbations show similar features, see Figure 6. The initial model in central Asia at 50 km depth shows faster wave speeds caused primarily by thick, cold lithosphere. Further to the south, into the Zagros Mountains where a large amount of continental deformation and crustal thickening is occurring, the wave speeds are substantially slower. This Asian north-to-south, fast-to-slow wave speed pattern in the initial model is mirrored in the second model iteration, right panel Figure 5. Similar behavior was identified in other finite-frequency tomography experiments (Montelli et al., 2004). Wave speed perturbations in the initial model are amplified when using sensitivity kernels based on a finite-frequency approach rather than an approximation, either classical ray theory or surface wave sensitivities kernels.

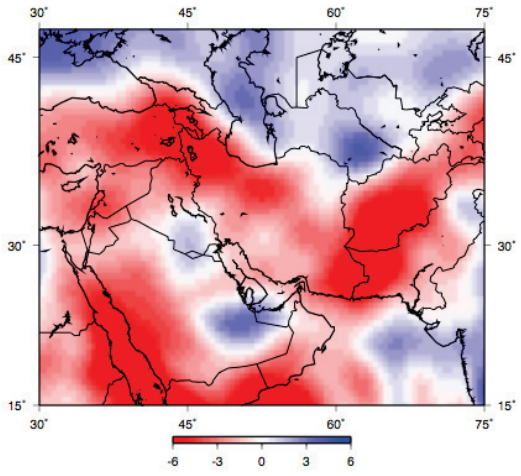

Figure 6. Initial Model shear wave speed variations +- 6% compared to the average value at 50 km depth.

Updates to the model also include density and compressional components. Compressional updates are shown in Figure 7; density is not shown. The initial 3D compressional wave speed model was scaled in the initial model from the 3D shear wave speed by a constant factor. Shear wave speeds in S2.9EA were derived from a large number of Love, Rayleigh, and shear body waves and was not directly constrained by seismic data. A comparison between the compressional adjoint results and the initial model can be difficult as the ratio between shear and compressional wave speeds can vary due to

chemistry. All adjoint iterations for compressional wave speeds show a much slower upper mantle beneath much of the Middle East than indicated by S2.9EA. Updates to the model at long wavelengths for these initial iterations are

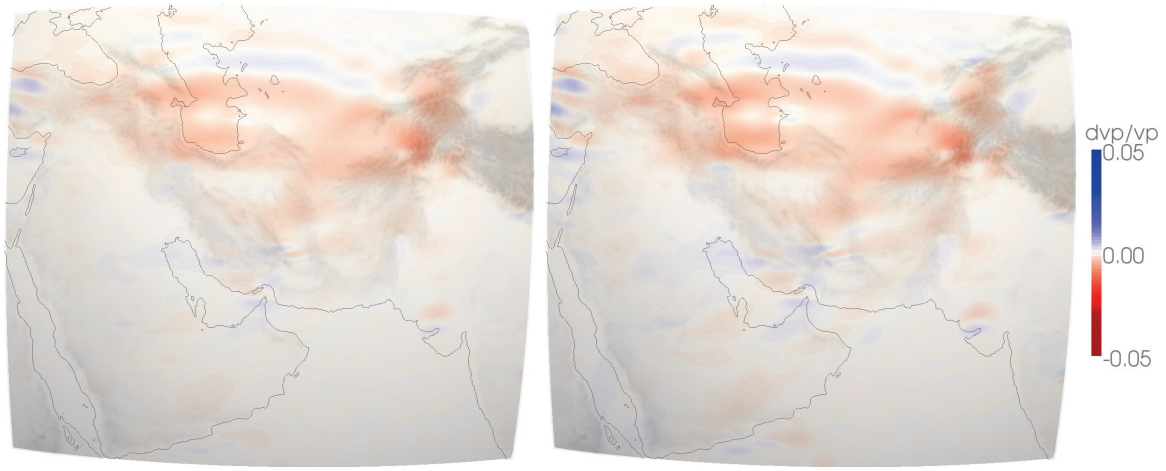

Figure 7. Compressional wave speed updates, same as for Figure 5.

predominately controlled by Rayleigh waves (shear and compressional surface wave) as the initial S2.9EA model fit the Love waves (shear only surface waves) better.

CONCLUSIONS AND RECOMMENDATIONS

Initial adjoint iterations to update a wave speed model of the Middle East have shown improvements to the model based on data / synthetic comparisons and expected behavior when introducing a finite-frequency tomographic approach. Before iterations began, a seismic waveform database with ~200 reinterpreted sources in the Middle East was compiled to avoid the mapping of source errors into wave speed structure. All sources in the database agree with previously published solutions and between the methodologies used: CAP (Zhao and Helmberger, 1994), teleseismic (Kikuchi and Kanamori, 1982) and a CMT inversion (Liu et al., 2004). Initial comparisons between data and synthetics computed from the initial 3D model S2.9EA (Kustowski et al., 2008) at 25 seconds and longer show reasonable agreement and a general improvement over the 1D PREM model (Dziewonski and Anderson, 1981).

To further improve the fit between data and synthetics, the adjoint inversion methodology was implemented to iteratively update the 3D wave speed model (Tromp et al., 2005). Following an initial set of iterations, the wave speed model was updated in a manner consistent with the finite-frequency tomographic techniques and the constraints on the initial wave speed model. Regions of wave speed perturbations have increased in magnitude from the initial to the second iteration as physics of wave propagation were incorporated into the inversion; see, e.g., the northern portion of the model in stable Asia (Figure 5, shear component). Compressional wave speed estimates also improved from increased use of Rayleigh waves and relaxing constraints between shear and compressional wave speeds. Our recommendations for a robustly constrained 3D wave speed model in the Middle East include using quality controlled seismic waveform data from well-constrained sources and use of a physics based tomographic technique to improve upon existing 3D models.

REFERENCES

Dziewonski, A., and D. Anderson (1981). Preliminary reference Earth model, *Phys. Earth. Planet. Int.* 25: 297–356.

Kikuchi, M., and H. Kanamori (1982), Inversion of complex body waves, *Bull. Seismol. Soc. Am.* 72: (2), 491–506.

Komatitsch, D., and J. Tromp (1999). Introduction to the spectral-element method for 3-D seismic wave propagation, *Geophys. J. Int.* 139: 806–822.

Kustowski, B., G. Ekstrom, and A. Dziewonski (2008). The shear-wave velocity structure in the upper mantle beneath Eurasia, *Geophys. J. Int.* 174: 978–992, 10.1111/j.1365-246X.2008.03865.x.

Liu, Q., J. Polet, D. Komatitsch, and J. Tromp (2004). Spectral-Element Moment Tensor Inversions for Earthquakes in Southern California, *Bull. Seismol. Soc. Am.* 94: (5), 1748–1761, 10.1785/012004038.

Maggi, A., C. Tape, M. Chen, D. Chao, and J. Tromp (2009). An Automated time-window selection algorithm for seismic tomography, *Geophys. J. Int.* 178: (1), 257–281, 10.1111/j.1365-246X.2009.04099.x.

Montelli, R., G. Nolet, F. Dahlen, G. Masters, E. Engdahl, and S. Hung (2004). Finite-Frequency Tomography Reveals a Variety of Plumes in the Mantle, *Science* 303: (5656), 338–343.

Tape, C., Q. Liu, A. Maggi, and J. Tromp (2009). Adjoint tomography of the Southern California crust, *Science*, 325: 988–992.

Tromp, J., C. Tape, and Q. Liu (2005). Seismic tomography, adjoint methods, time reversal and banana-doughnut kernels, *Geophys. J. Int.* 160: (1), 195–216.

Zhao, L., and D. Helmberger (1994). Source estimation from broadband regional seismograms, *Bull. Seismol. Soc. Am.* 84: (1), 91–104.